Inclined-aligned ZnO nanorod array for self-powered all-scenario underwater weak light detection and optical communication

Yuan Zhang, Junxin Zhou, Wenhui Li, Jiaming Liu, Xinghan Li, Sihan Yuan, Xinai Li, PingAn Hu, Wei Feng*

Y. Zhang, J. Zhou, W. Li, J. Liu, X. Li, S. Yuan, X Li, Prof. W. Feng

College of Chemistry, Chemical Engineering and Resource Utilization, Northeast Forestry University, Harbin 150040, China

Email: wfeng@nefu.edu.cn

Prof. P. Hu

Key Laboratory of Micro-Systems and Micro-Structures Manufacturing, Harbin Institute of Technology, Harbin 150001, China

1 Experimental section

1.1 Materials and characterization

1.1.1 Materials

Hexamethylenetetramine ($C_6H_{12}N_4$,99%), zinc nitrate hexahydrate ($Zn(NO_3)_2·6H_2O$, 99%), Potassium hydroxide (KOH,99%), sulfuric acid (H_2SO_4,99%), sodium chloride (NaCl,99%), sodium bicarbonate ($NaHCO_3$,99%), potassium chloride (KCl,99%), magnesium chloride hexahydrate ($MgCl_2·6H_2O$,99%), calcium chloride ($CaCl_2$,99%), fluorine-doped tin dioxide (FTO) glass, FTO needs to be ultrasonically cleaned with ethylene glycol, acetone, ethanol, and deionized water for 10 min.

1.1.2 Characterization

The Crystal structure and purity of the ZnO were measured by X-ray diffraction (XRD, RIGAKU Smartlab SE with Cu Kα radiation (λ = 1.5406 Å)). The Crystallinity and morphology of ZnO were measured by transmission electron microscopy (TEM, FEI, Tecnai TF20) and scanning electron microscopy (SEM, Thermofisher Apreo 2C). UV–vis diffuse reflection spectra were obtained by a UV-3600 Shimadzu UV-vis-NIR absorbance spectrometer.

1.2 Preparation of ZnO inclined nanorod array

0.742 g of $Zn(NO_3)_2·6H_2O$ and 0.35 g of $C_6H_{12}N_4$ were dissolved in 50 ml of deionized water and stirred at room temperature for 20 min. 25 ml of precursor solution was put in a 50 ml polytetrafluoroethylene-lined stainless steel autoclave, and two pieces of FTO (conductive side down) were placed in the polytetrafluoroethylene-lined stainless steel autoclave for reaction at 90 °C for 0.5, 1, 3, 5, or 10 h, named as ZnO-0.5, ZnO-1, ZnO-3, ZnO-5, and ZnO-10, respectively. All ZnO samples were annealed in air at 600 °C for 30 min.

1.3 Electrochemical measurements

The test system was a three-electrode system, with the prepared ZnO INRA as the working electrode, a saturated calomel electrode functioning as the reference electrode, and a platinum sheet as the counter electrode. 0.1 M KOH, 5×10^{-6} M H_2SO_4, and simulated seawater are electrolytes, respectively. LED light with different wavelengths and power densities as the irradiated light sources (see Table S1 of the Supporting Information for more information), and the light intensities were measured using an optical power meter (Daheng Optics GCI-08) in air. The PEC tests were conducted in a dark box to eliminate the influence of environmental lights.

Exploration of optimal synthesis conditions of ZnO INRA

Using the hydrothermal method, ZnO INRA was successfully synthesized on FTO with optimized synthesis parameters[1]. The transformation of the height of ZnO INRA from nanometers to the micron scale was achieved by controlling the hydrothermal times. Figure S1a is an SEM image of blank FTO. It can be observed that the surface of the FTO is not smooth and includes lots of pinnacles, thus providing nucleation sites for the growth of ZnO INRA without other templates. Figures 1a and S2a-d show SEM images of ZnO hydrothermal times of 0.5, 1, 3, 5, and 10 h, respectively. ZnO INRA with different scales and coverage rates is obtained by controlling the hydrothermal time. Figure 1b and S2e-h show the cross-section SEM images of 0.5, 1, 3, 5, and 10 h, respectively. It can be seen from Figure S1b that the thickness of the FTO conductive layer is about 473.8 nm. The height of ZnO INRA increases with the increase in hydrothermal time (0.92 to 3.53 μm). As show in Figure 1b, Figure S1h, and Figure S3, when the hydrothermal time is 10 h, the height of ZnO-10 INRA is about 3.53 μm and diameter is about 0.51 μm, compared with ZnO-5 (the height is about 3.37 μm and diameter is about 0.49 μm), the height and diameter of ZnO-10 nanorods are almost unchanged.

To investigate the effects of different hydrothermal times on the photoresponse, the current density-time (*J*-t) curves were tested with 365 nm light under different optical power intensities (more details in Table S1), as shown in Figure S4a. The Jph increases with increasing hydrothermal time (more details in Table S2). When the hydrothermal time is 5 h, it exhibits the optimal photoresponse (ZnO-5 and ZnO-10 have almost equal J_{ph}). Therefore, 5 h is the optimal synthesis time. Cyclic voltammetry

(CV) tests were carried out on these samples to further explain the reasons for the increased photoresponse. The area of the CV curve represents the electrochemically active surface area (ECSA)[2], and the larger the ECSA leads to higher the photoresponse3. As shown in Figure S4b, with the increase of hydrothermal time, the ECSA increases, and ZnO-5 and ZnO-10 have similar ECSA. As shown in Figure S4c, after the hydrothermal reaction time exceeded 0.5 hours, ZnO synthesized at different times exhibited similar absorption peak, and the peak intensities of ZnO-5 and ZnO-10 were comparable.

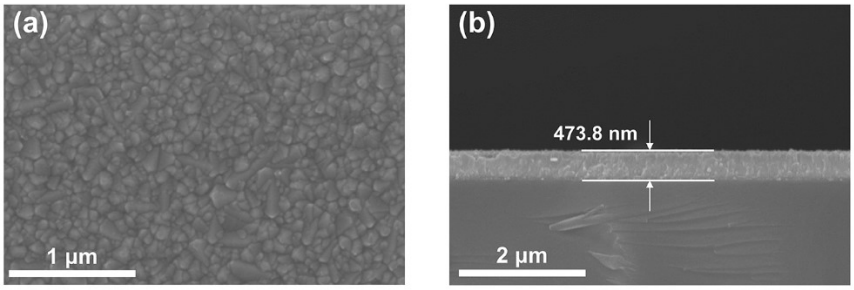

Figure S1. (a) SEM of FTO. (b) SEM cross-section of FTO

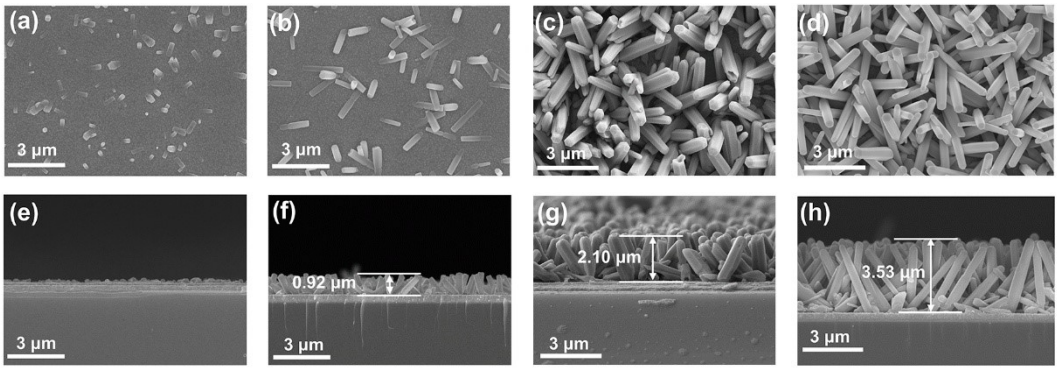

Figure S2. Top-view SEM images of ZnO INRA at 0.5, 1, 3, and 10 h hydrothermal times: (a) ZnO-0.5, (b) ZnO-1, (c) ZnO-3, and (d) ZnO-10. Cross-section SEM images of ZnO INRA at 0.5, 1, 3, and 10 h synthesis times: (e) ZnO-0.5, (f) ZnO-1, (g) ZnO-3, and (h) ZnO-10.

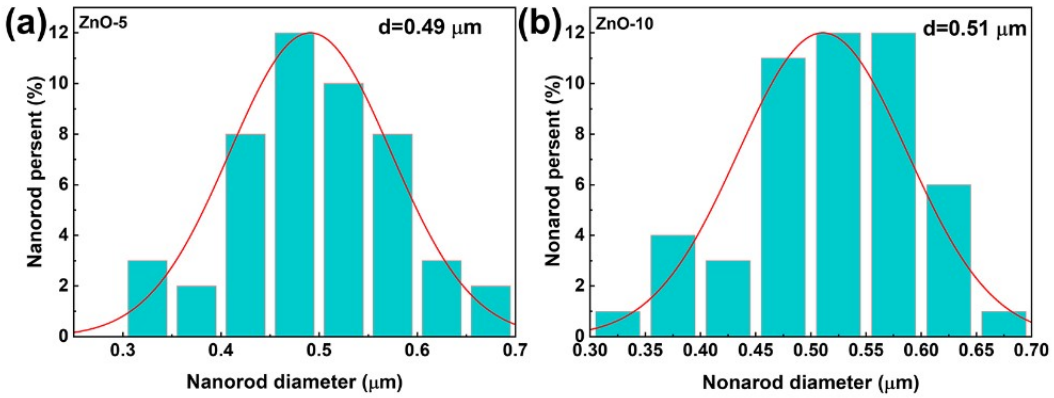

Figure S3. (a) The nanorod diameter of ZnO-5. (b) The nanorod diameter of ZnO-10.

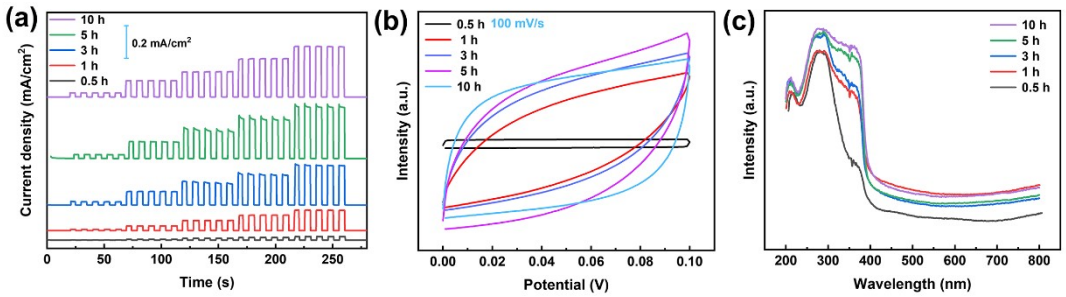

Figure S4. (a) Comparison of J_{ph} at different synthesis times in 0.1 M KOH solution. (b) CV curves for different synthesis times in 0.1 M KOH solution. (c) UV-vis DRS for different synthesis times.

Table S1. The light power intensity for various wavelengths.

Light (nm) \ P (mW/cm^2)	I	II	III	IV	V
365	0.089	0.43	0.81	1.23	1.58
455	0.91				

Table S2. The calculated J of various ZnO INRA PEC UV photodetectors illuminated

by different synthesis conditions at various *P* in 0.1 M KOH.

J_{ph} (μA/cm^2) / Samples	I	II	III	IV	V
0.5	1.1	4.5	10	15.9	21.1
1	6.4	28.5	61.8	95.1	124.7
3	19.3	84.3	142.9	184.1	241.1
5	24.9	98.4	162.5	238.2	317.6
10	24.4	99.7	154.9	233.7	314.9

Table S3. The calculated *R* of various ZnO PEC UV photodetectors illuminated by different synthesis conditions at various *P* in 0.1 M KOH.

J_{ph} (μA/cm^2) / Samples	I	II	III	IV	V
0.5	12.4	10.5	12.5	13.3	13.2
1	71.9	66.3	77.3	79.3	77.9
3	216.9	196.0	178.6	153.4	150.7
5	279.8	228.8	200.6	182.4	180.9
10	274.2	231.9	193.6	194.8	196.8

Table S4. The calculated *D** of various ZnO PEC UV photodetectors illuminated by

different synthesis conditions at various *P* in 0.1 M KOH.

Samples \ *D**(10^{11} Jones)	I	II	III	IV	V
0.5	3.2	2.7	3.3	3.5	3.4
1	18.7	17.4	20.1	20.7	20.3
3	56.5	51.0	46.5	39.9	39.2
5	72.8	59.6	52.9	47.5	41.7
10	71.4	60.4	50.4	50.7	51.3

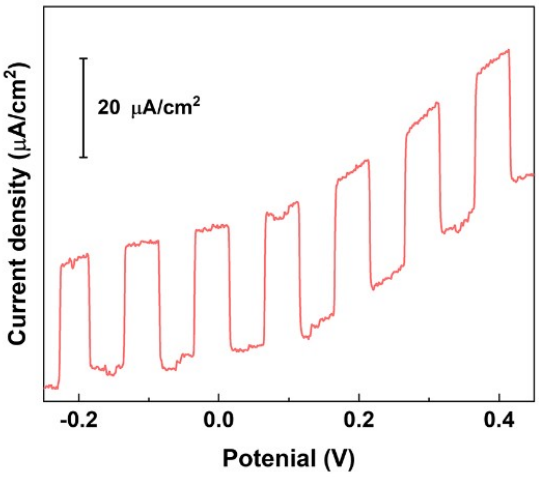

Figure S5. Linear sweep voltage (LSV) curve of ZnO-5 PEC UV photodetector under pulsed 365 nm (0.089 mW/cm^2) light irradiation.

Table S5. The calculated J_{ph} of ZnO INRA PEC UV photodetectors in different

solutions and temperatures.

J_{ph} (μA/cm^2) / Temperature (°C)	KOH	Seawater	H_2SO_4
5	24.4	10.8	6.7
25	24.9	13.6	6.9
45	25.3	13.7	8.4

Table S6. The calculated *R* of ZnO INRA PEC UV photodetectors in different solutions and temperatures.

R (mA/W) / Temperature (°C)	KOH	Seawater	H_2SO_4
5	273.7	121.7	75.1
25	279.8	152.4	77.4
45	284.4	153.5	94.9

Table S7. The calculated *D** of ZnO INRA PEC UV photodetectors in different solutions and temperatures.

*D**(10^{11} Jones) / Temperature (°C)	KOH	Seawater	H_2SO_4
5	71.2	31.6	19.5
25	72.8	39.6	20.1
45	73.9	39.9	24.7

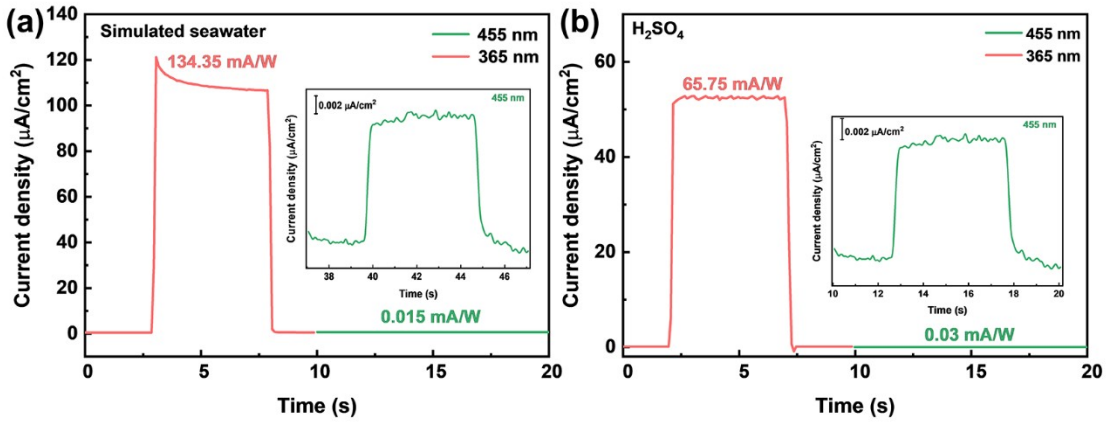

Figure S6. Corresponding R of ZnO INRA PEC UV photodetector irradiated at 365 (level III) and 455 nm (0.91 mW/cm^2) in (a) seawater and (b) H_2SO_4 solution.

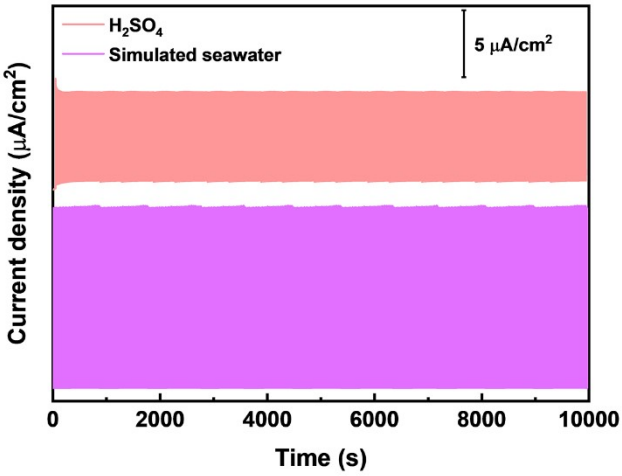

Figure S7. Stability measurements of ZnO INRA PEC UV photodetectors in seawater and 5×10^{-6} M H_2SO_4 solution.

Table S8. Performance comparison of recently reported PEC UV PDs

Materials	Measurement conditions	UV/Visible	Light (nm)	*R* (mA/W)	*Tr*/*Td* (s)	Ref.
ZnO INRA	0.1 M KOH	10030.5	365	279.8	0.005/0.022	This work
ZnO INRA	Simulated seawater	8956.7	365	152.4	0.004/0.024	This work
ZnO INRA	5×10^{-6} M H_2SO_4	2191.8	365	77.4	0.02/0.03	This work
In_2O_3 NAs	1 M KOH	1319	254	86.15	0.015/0.018	4
In_2O_3 MR	0.01 M Na_2SO_4	20.77	365	21.19	0.5/1.1	5
Diamond single crystal	5 mM H_2SO_4	-	213	20	0.05/0.038	6
In_2O_3 NCF	1 M KOH	13.5	365	44.43	0.02/0.03	7

Ga−In OAs	0.01 M Na_2SO_4	262.45	254	50.04	0.45/0.38	8
ZnAl MMO	0.01 M KOH	1088.8	365	46.82	0.018/0.035	9
AlGaN NWs	0.01 M H_2SO_4	-	254	48.8	0.083/0.019	10
In_2O_3 NSs	Distilled water,0 V	1567	365	172.36	0.8/2.2	11
ZnS NPF	0.1 M Na_2SO_4	-	254	241.71	0.015/0.015	12
ZnS SSNWs	0.5 M Na_2SO_4	-	265	33.7	-	13
ZnAl-LDH	0.01 M KOH	1037	254	29.25	0.1/0.1	14
(Al,Ga)N NWs	Distilled water	485	310	84.2	6.2/6.2	15
SnO_2 NSs	1 M Na_2SO_4	120	254	269.4	0.6/0.8	16
Pt/GaN NWs	0.5 M H_2SO_4	181.4	365	42.4	-	17
Pt/AlGaN NWs	0.5 M H_2SO_4	-	254	45	0.047/0.02	18
GaN/IrOx NWs	0.01 M PBS	1166.7	365	110.1	＜0.001	19
ZnO NWs	0.5 M Na_2SO_4	-	365	74.61	0.159/0.15	20
ZnO NWs	NaOH, PH=13	-	365	47.4	0.022/0.049	21
ZnO NWs	I^-/I^{3-}	-	360	50	0.15/0.05	22
ZnO/Cu_2O NWs	0.5 M Na_2SO_4	3	355	19.3	0.14/0.36	23
ZnO/ZnS NAs	8 mM H_2PtCl_4	-	340	56	0.04	24

NAs: nanosheet arrays; MRs: Microrods; NCF: nanocube film; OAs: oxide alloys; MMO: mixed metal oxide; NWs: nanowires; NSs: nanosheet arrays; NPF: nanoparticle film; SSNWs: single-unit-cell semiconductor nanowires; NSs: nanosheet arrays.

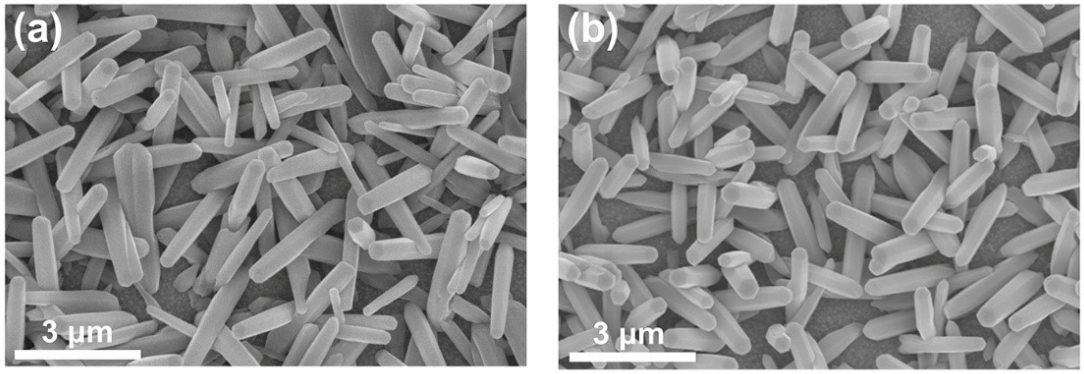

Figure S8. (a) SEM image of ZnO-5 nanorods after multi-cycle stability. (b) SEM image of ZnO-5 nanorods after long-term stability.

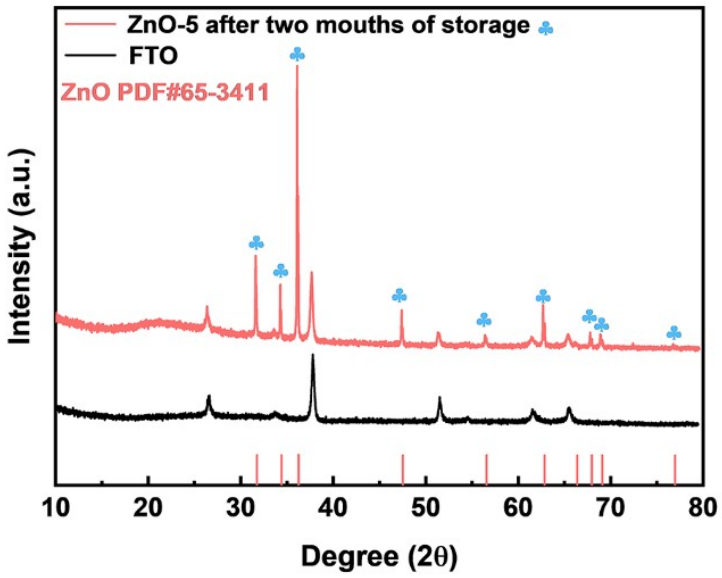

Figure S9. XRD patterns of ZnO-5 after two months of storage.

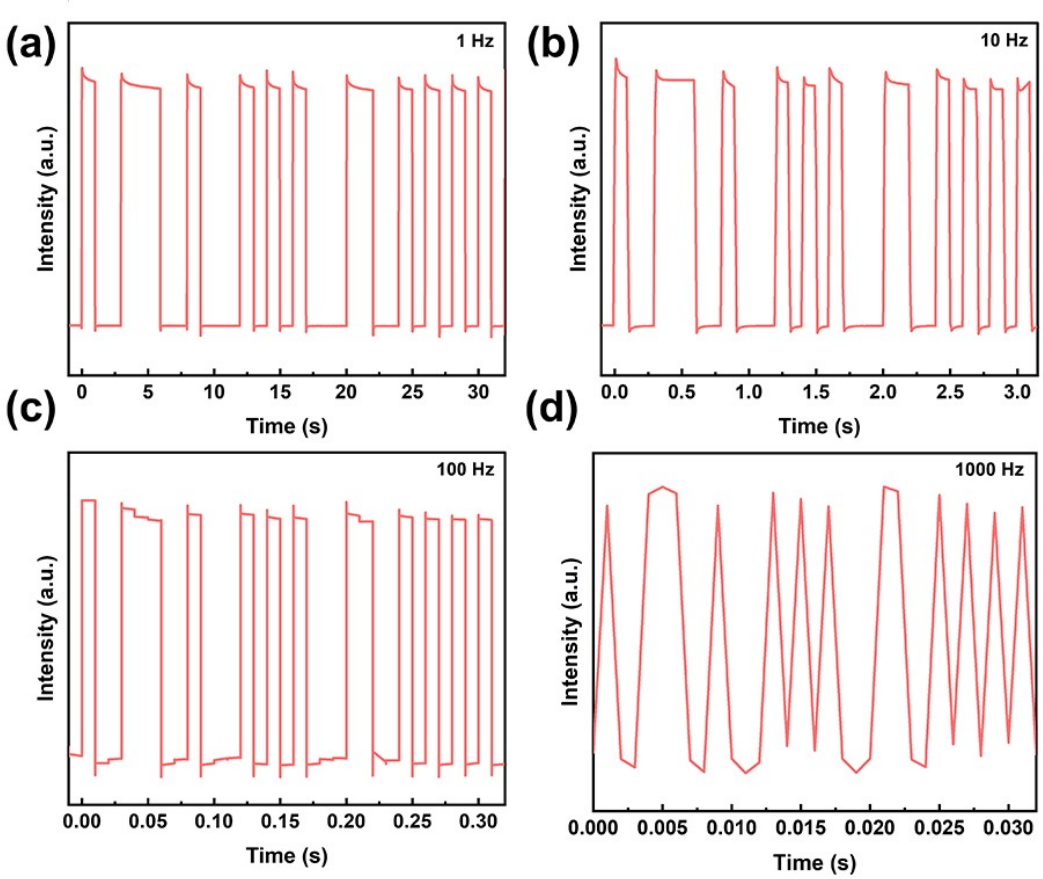

Figure S10. (a–d) The response curves at transmitting frequencies of 1, 10, 100, and 1000 Hz in 0.1 M KOH.

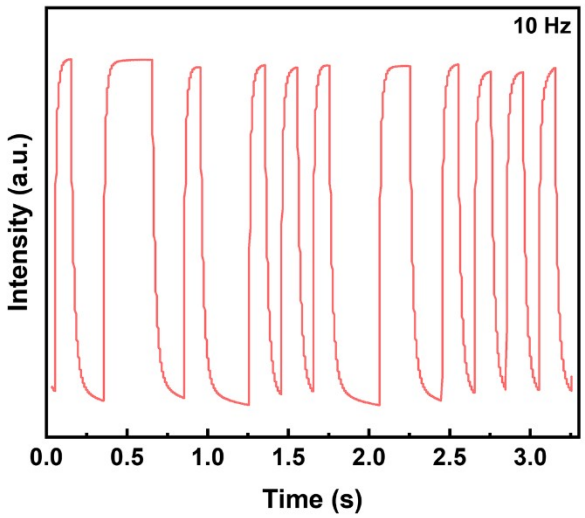

Figure S11. The response curves at a transmitting frequency of 10 Hz in 5×10^{-6} M H_2SO_4.

References

1. Kang, Z.; Yan, X.; Wang, Y.; Zhao, Y.; Bai, Z.; Liu, Y.; Zhao, K.; Cao, S.; Zhang, Y., Self-powered photoelectrochemical biosensing platform based on Au NPs@ZnO nanorods array. *Nano Research* **2015,** *9* (2), 344-352.

2. Raciti, D.; Livi, K. J.; Wang, C., Correction to Highly Dense Cu Nanowires for Low-Overpotential CO_2 Reduction. *Nano Letters* **2016,** *16* (10), 6716-6716.

3. Wang, Y.; Zhang, A.; Shao, Z.; Yu, H.; Xu, Y.; Liu, X.; Cui, M.; Gao, F.; Hu, P.; Feng, W., High-Performance Se-Based Photoelectrochemical Photodetectors Via in Situ Grown Microrod Arrays. *Advanced Optical Materials* **2022,** *10* (24), 2201926.

4. Zhang, N.; Gao, X.; Guan, H.; Sun, S.; Liu, J.; Shao, Z.; Gao, Q.; Zhang, Y.; Sun, R.; Yang, G.; Gao, F.; Feng, W., Three-dimensional porous In_2O_3 arrays for self-powered transparent solar-blind photodetectors with high responsivity and excellent spectral selectivity. *Nano Research* **2023,** *17* (5), 4471-4477.

5. Cui, M.; Shao, Z.; Qu, L.; Liu, X.; Yu, H.; Wang, Y.; Zhang, Y.; Fu, Z.; Huang, Y.; Feng, W., MOF-Derived In_2O_3 Microrods for High-Performance Photoelectrochemical Ultraviolet Photodetectors. *ACS Applied Materials & Interfaces* **2022,** *14* (34), 39046-39052.

6. Cheng, L.; Wu, Y.; Cai, W.; Zheng, W., Diamond immersion photodetector for 213 nm deep-ultraviolet photodetection. *Materials Today Physics* **2023,** *36*, 101164.

7. Zhang, N.; Cui, M.; Zhou, J.; Shao, Z.; Gao, X.; Liu, J.; Sun, R.; Zhang, Y.; Li, W.; Li, X.; Yao, J.; Gao, F.; Feng, W., High-Performance Self-Powered Photoelectrochemical Ultraviolet Photodetectors Based on an In_2O_3 Nanocube Film. *ACS Applied Materials & Interfaces* **2024,** *16* (15), 19167-19174.

8. Shao, Z.; Qu, L.; Cui, M.; Yao, J.; Gao, F.; Feng, W.; Lu, H., Achieving High-Performance Self-Powered Visible-Blind Ultraviolet Photodetection Using Alloy Engineering. *ACS Applied Materials & Interfaces* **2023,** *15* (37), 43994-44000.

9. Sun, S.; Li, W.; Zhang, Y.; Gao, Q.; Zhang, N.; Qin, Y.; Feng, W., Mixed Metal Oxide

Heterojunction for High-Performance Self-Powered Ultraviolet Photodetection. *Small* **2024**, *21* (4), 2407107.

10. Wang, D.; Huang, C.; Liu, X.; Zhang, H.; Yu, H.; Fang, S.; Ooi, B. S.; Mi, Z.; He, J. H.; Sun, H., Highly Uniform, Self-Assembled AlGaN Nanowires for Self-Powered Solar-Blind Photodetector with Fast-Response Speed and High Responsivity. *Advanced Optical Materials* **2020,** *9* (4), 2000893.

11. Zhang, M.; Yu, H.; Li, H.; Jiang, Y.; Qu, L.; Wang, Y.; Gao, F.; Feng, W., Ultrathin In_2O_3 Nanosheets toward High Responsivity and Rejection Ratio Visible-Blind UV Photodetection. *Small* **2022,** *19* (1), 2205623.

12. Zhang, Y.; Shao, Z.; Zhou, J.; Sun, S.; Sun, R.; Zhang, N.; Liu, J.; Gao, X.; Hu, P.; Feng, W., Vacancy Engineering Optimizing Solid/Liquid Interfacial Properties for Boosting Self-Powered Solar-Blind Photodetection. *Advanced Optical Materials* **2024,** *12* (34), 2401639.

13. Li, D.; Hao, S.; Xing, G.; Li, Y.; Li, X.; Fan, L.; Yang, S., Solution Grown Single-Unit-Cell Quantum Wires Affording Self-Powered Solar-Blind UV Photodetectors with Ultrahigh Selectivity and Sensitivity. *Journal of the American Chemical Society* **2019,** *141* (8), 3480-3488.

14. Sun, S.; Zhang, Y.; Gao, Q.; Zhang, N.; Hu, P.; Feng, W., ZnAl-LDH film for self-powered ultraviolet photodetection. *Nano Materials Science* **2024**, *7* (3), 377-382.

15. Jiang, M.; Zhao, Y.; Bian, L.; Yang, W.; Zhang, J.; Wu, Y.; Zhou, M.; Lu, S.; Qin, H., Self-Powered Photoelectrochemical (Al,Ga)N Photodetector with an Ultrahigh Ultraviolet/Visible Reject Ratio and a Quasi-Invisible Functionality for 360° Omnidirectional Detection. *ACS Photonics* **2021,** *8* (11), 3282-3290.

16. Yu, H.; Qu, L.; Zhang, M.; Wang, Y.; Lou, C.; Xu, Y.; Cui, M.; Shao, Z.; Liu, X.; Hu, P.; Feng, W., Achieving High Responsivity of Photoelectrochemical Solar-Blind Ultraviolet Photodetectors via Oxygen Vacancy Engineering. *Advanced Optical Materials* **2022,** *11* (4), 2202341.

17. Fang, S.; Wang, D.; Wang, X.; Liu, X.; Kang, Y.; Yu, H.; Zhang, H.; Hu, W.; He, J. H.; Sun, H.; Long, S., Tuning the Charge Transfer Dynamics of the Nanostructured GaN Photoelectrodes for Efficient Photoelectrochemical Detection in the Ultraviolet Band. *Advanced Functional Materials* **2021,** *31* (29), 2103007.

18. Wang, D.; Liu, X.; Fang, S.; Huang, C.; Kang, Y.; Yu, H.; Liu, Z.; Zhang, H.; Long, R.; Xiong, Y.; Lin, Y.; Yue, Y.; Ge, B.; Ng, T. K.; Ooi, B. S.; Mi, Z.; He, J.-H.; Sun, H., Pt/AlGaN Nanoarchitecture: Toward High Responsivity, Self-Powered Ultraviolet-Sensitive Photodetection. *Nano Letters* **2020,** *21* (1), 120-129.

19. Fang, S.; Li, L.; Wang, D.; Chen, W.; Kang, Y.; Wang, W.; Liu, X.; Luo, Y.; Yu, H.; Zhang, H.; Memon, M. H.; Hu, W.; He, J. H.; Gong, C.; Zuo, C.; Liu, S.; Sun, H., Breaking the Responsivity-Bandwidth Trade-Off Limit in GaN Photoelectrodes for High-Response and Fast-Speed Optical Communication Application. *Advanced Functional Materials* **2023,** *33* (37), 2214408.

20. Tang, Q.; Tan, G.; Zhang, H.; Li, H.; Xiong, Y.; Pang, D.; Ye, L.; Fang, L.; Kong, C.; Li, W., Enhanced photoresponse of self-powered ZnO-based photoelectrochemical-type UV photodetectors via Ga-doping for optical communication application. *Journal of Alloys and Compounds* **2024,** *972*, 172864.

21. Ji, Y.; Wu, L.; Liu, Y.; Yang, Y., Chemo-phototronic effect induced electricity for enhanced self-powered photodetector system based on ZnO nanowires. *Nano Energy* **2021,** *89*, 106449.

22. Xie, Y.; Li, H.; Zhang, D.; Zhang, L., High-performance quasi-solid-state photoelectrochemical-type ultraviolet photodetector based on ZnO nanowire arrays. *Vacuum* **2019,** *164*, 58-61.

23. Bai, Z.; Zhang, Y., Self-powered UV–visible photodetectors based on ZnO/Cu_2O

nanowire/electrolyte heterojunctions. *Journal of Alloys and Compounds* **2016,** *675*, 325-330.
24. Lin, H.; Wei, L.; Wu, C.; Chen, Y.; Yan, S.; Mei, L.; Jiao, J., High-Performance Self-powered Photodetectors Based on ZnO/ZnS Core-Shell Nanorod Arrays. *Nanoscale Research Letters* **2016,** *11* (1), 420.